Materials Research Express

PAPER

# Evaluation of the particle geometry and interphase influence on the filler-matrix debonding process

To cite this article: E Pérez and B Lauke 2019 *Mater. Res. Express* **6** 085341



Materials Research Express

PAPER

# Evaluation of the particle geometry and interphase influence on the filler-matrix debonding process

RECEIVED
15 April 2019

REVISED
15 May 2019

ACCEPTED FOR PUBLICATION
5 June 2019

PUBLISHED
14 June 2019

E Pérez[1,2,4] and B Lauke[3]

[1] National Scientific and Technical Research Council (CONICET), Av. Rivadavia 1917, (C1033AAJ), Buenos Aires, Argentina
[2] Plastics Research and Development Center, National Institute of Industrial Technology (INTI-Plásticos), Av. Gral. Paz 5445, (B1650KNA), San Martín, Buenos Aires, Argentina
[3] Private citizen, Germany
[4] Author to whom any correspondence should be addressed.

**E-mail:** eperez@inti.gob.ar **and** ablauke@web.de

**Keywords:** polymer-matrix composites (PMCs), debonding, interface/interphase, analytical modelling, numerical modelling

## Abstract

Incorporation of rigid fillers into polymer matrices represents a widely used technique to obtain improved performance. The mechanical behavior finally obtained is closely related to a wide range of involved factors (filler type and size, internal structure, filler-matrix interaction, among others) and to activated dissipative mechanisms (debonding, plastic void growth, crazing, matrix yielding, etc). In this work, a debonding strength approach was applied for rigid particles (spherical, elliptical and fiber) surrounded by an interphase. The effect of interphase mechanical properties and thickness on the debonding process was investigated. The obtained results suggested a significant influence of the transition rigidity. In general, stiffer interphases promoted higher critical strength values. On the other hand, particle surrounded by a softer transition region displayed higher dissipated energy for all examined particle, except for spheres.

## 1. Introduction

The processing of polymer based composites reinforced with rigid particles represents a possible way to obtain materials with enhanced performance. The mechanical properties finally observed has been related to the load transfer capability (from the polymer matrix to the filler) and to the effective activation of dissipative energy mechanisms [1–7]. The particle size effect has been widely discussed for which the most noticeable variations were detected on the nano-scale. This kind of behavior was related to the large surface/volume ratio of the incorporated fillers [8–10]. In addition, the composite performance is not exclusively determined by the filler size and a large variety of particle characteristics are also involved as: shape, chemical composition, impurities, surface energy, filler-matrix interaction, among others [1, 3, 8, 11]. Particularly, an interphase region could be formed around the rigid particle by the restricted polymer chains mobility meaning that the matrix mechanical properties are locally different to the bulk ones. This transition zone could be induced and/or affected by filler surface treatments or coatings, incorporation of coupling agents or modified polymers, among others [11–13]. Although, the relevance of the interphase has been well established, the related data actually available are not enough to clearly define its dimensions, mechanical properties and their law of variation across the thickness [8, 14, 15]. For this reason, in mechanical properties modeling, the interphase is neglected or some arbitrary definitions are required.

Theoretical models have been proposed to analyze damage and failure mechanisms of composite materials [13, 16–18]. The analytical solutions are stress or energy based criteria which lead sometimes to contradictory or unrealistic results. In a general way, Leguillon [19] analyzed both the energy and the stress conditions for crack onset suggesting that both criteria are clearly required for accurate predictions. Based on the Finite Fracture Mechanics (FFM) approach, debonding stress solutions have been proposed by Chen *et al* [20] and Zappalorto *et al* [15] for spherical symmetric situations without and with a constant interphase region, respectively. Chen

*et al* reported lower energy dissipation for nano-sized fillers while the opposite tendency can be expected for debonding stress [20]. Zappalorto *et al* showed the relevant effect of the interphase/matrix elastic properties ratio (from 0.25 to 4) where a soft transition displayed lower debonding values compared to stiffer ones. On the other hand, the thickness displayed only a marginal influence with interphase/particle dimension ratio lower than 2 [15]. In addition, a general approach was published for the debonding stress calculation which is not limited to spherical fillers [21]. The proposed solution was applied for different particle shapes neglecting the interphase. The most remarkable conclusion was that, cubic and prolate particles can be easily analyzed as spherical situations [21]. It can be highlighted that, the reported expressions in [15] and [20] predicts a sharp increase on the critical stress as the particle dimensions are reduced. These results suggest that, the debonding process could be hardly achieved by incorporation of nano-fillers. But, this theoretical prediction lays in contrast with reported experimental performance of polymer based nanocomposites [22–25]. On the other hand, the proposed solution in [21] suggests that, debonding is close related to the displacement field of the polymer matrix after debonding. Taking into account the elastic-plastic behavior of the matrix, it is possible to satisfy the critical condition without stress increments. Unfortunately, none of the theoretical predictions could been experimentally verified yet, due to that the development of some specific testing and/or characterization procedures are still required. In general, the available experimental data represents an overview not easily related with the theoretical models. Particularly, mechanical tests can be analyzed through experimental curves, characteristic parameters and fracture surfaces allowing to describe the composites performance [25–28]. But, they do not represent a detailed description of any single particle along the whole loading process until failure. In this way, multi-scale mechanical tests performed under *in situ* observations (high resolution imaging, digital image correlation, microscopy) alongside additional measurements (acoustic emission, x-ray tomography, thermography, among others) and their correlations with modelling or numerical solutions look as promising experimental-theoretical procedures [28–32].

Williams [6] analyzed the polymer composite toughening due to plastic void growth around debonded particles. The composite toughness prediction is optimistic for small particles (lower than 10 nm), however not yet experimentally checked. This discrepancy has been explained by the effective filler dispersion and by the large plastic strain considered for modeling. Carraro *et al* [16] analyzed the relationship between damage mechanisms (debonding and matrix failure) and fiber radius defining three different regions. Into the first stage for very small radius, the matrix strength is the predominant factor. For the other two regions, particle debonding is the prevalent mechanism but it is driven by a transition from interface fracture toughness (energy driven) to interfacial strength (stress driven) as a function of the fiber radius. Salviato *et al* [8] analyzed the effect of the interface and the elastic properties of an interphase on the debonding process of nano-spheres. The interphase considered was 4 nm thick with an elastic modulus variation from 0.25 to 4 compared to the matrix. They reported a significant effect of the interphase properties while the surface stresses can be neglected. Dastgerdi *et al* [17] proposed a theoretical model for tensile behavior taking into account debonding of spherical reinforcements without interphase into a elasto-plastic matrix. They compared analytical results with experimental data and concluded that, the debonding damage should be considered to avoid theoretical discrepancies. Quaresiminin *et al* [14] proposed a multi-mechanism approach based on a multi-scale strategy. The developed model considered different energetic contributions (matrix toughness, particle debonding and plastic void growth) based on a nano-scale system composed by the polymer matrix, interphase and a spherical particle. The authors also discussed the lack of data related to the interphase characteristics, thus due to calculation requirements its properties (yield and strength equal to the matrix) and size were imposed. Based on the published data briefly described it can be suggested that the debonding process should be investigated taking into account different particle shapes (not exclusively spheres), interphase properties and thickness, interfacial energy and loading conditions.

In the present work, the previously published general approach [21] for debonding strength was applied for rigid particles (spherical, elliptical and fiber) surrounded by an interphase into the polymer matrix. In this way, the influence of the different particle geometry and interphase characteristics (mechanical properties and thickness) was directly compared. In addition, the debonding process was also analyzed in terms of strength, stress concentration and energetic contribution. On the other hand, the size limit of the proposed criterion was discussed.

## 2. Debonding strength approach

The general solution herein is derived for a single particle surrounded by the polymer matrix and considering the FFM approach [21]. The equilibrium of the system was determined before and after debonding. For these situations, it was assumed: (i) a constant hydrostatic stress remotely applied, (ii) particle perfectly bonded in the initial condition, (iii) debonding is determined by the normal component to the filler-matrix interface and (iv)

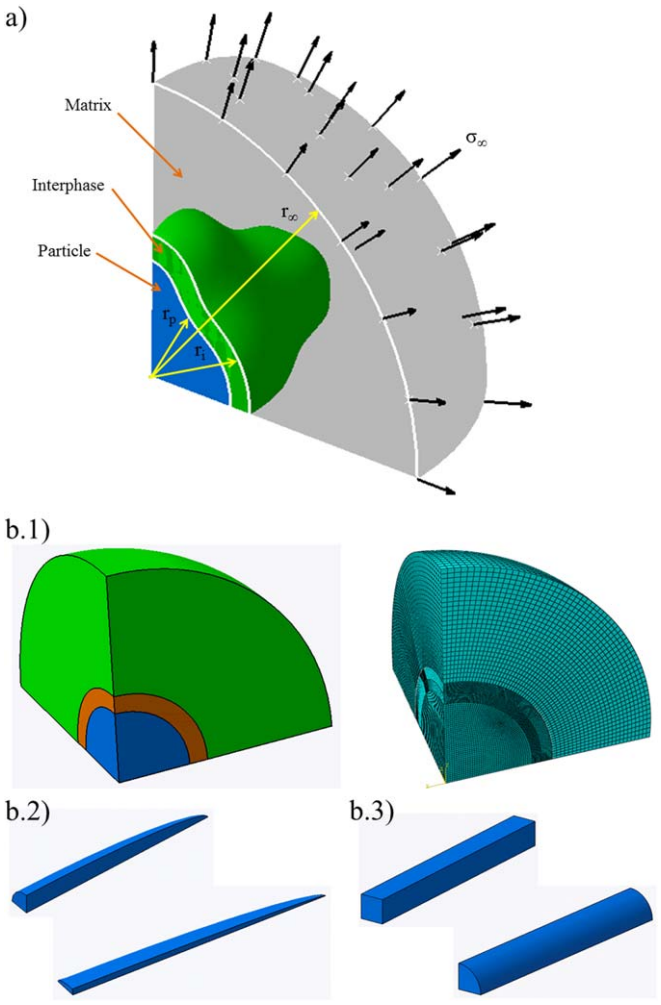


**Figure 1.** Description of the analyzed system: (a) particle, interphase and matrix under hydrostatic remote stress and (b) particle geometries (b.1 sphere and FEA mesh, b.2 ellipsoids, b.3 fibers).

fully particle debonding occurs when the critical condition is achieved. Under these assumptions and simplifications the following general solution was proposed [21]:

$$\sigma_{cr} = \frac{2\gamma \int dA}{\int u^{m}_{2(r_p)}\, dA} \tag{1}$$

where: $\sigma_{cr}$ is the critical normal strength, $\gamma$ is the interfacial fracture energy, $u^{m}_{2(r_p)}$ is the matrix displacement at the particle surface after debonding and $A$ is the debonded surface. In the following, due to the incorporation of the interphase (figure 1(a)) the required displacement value after debonding should be determined at the filler-interphase boundary.

### 2.1. Interphase and particle geometry considerations

In the previously published work, the transition region between matrix and particle was neglected, as a first simplified analyzing step. In the following sections an interphase is considered and its influence is discussed. The interphase thickness is assumed to be 0.25 and 0.5 of the particle shortest dimension while the elastic modulus was 0.25 and 4 compared to the polymer matrix. Similar characteristics were also used by other authors and these values were adopted for comparison [8, 15]. The materials of the components were considered as isotropic and linear elastic:

1. matrix: $E_m = 1.6$ GPa; $\upsilon_m = 0.4$
2. interphase: $\gamma = 0.01$ J m$^{-2}$; $E_i = (0.25; 4)^{*}E_m$; $\upsilon_i = 0.4$
3. particle: $E_p = 16$ GPa; $\upsilon_p = 0.2$

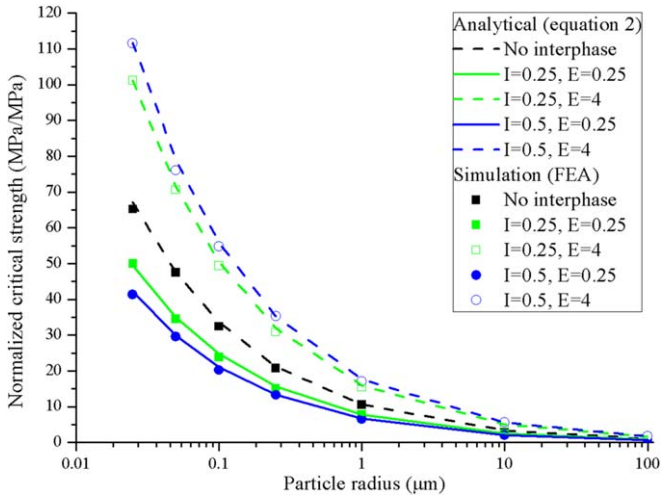


**Figure 2.** Normalized debonding stress values for spheres.

The general solution was applied for the following particle shapes (figure 1(b)) and semi-axis relationships: (i) sphere (a = b = c), (ii) ellipsoid (a = b, c/b = 10 and b/a = 4, c/b = 10) and (iii) fiber (a = b square cross-section, c/b = 10 and a = b circular cross-section, c/b = 10) in the size range of 0.01–100 $\mu$m for the inclusion shortest dimension. The filler geometries were defined based on the previously reported work for which the largest differences, compared to the spherical situation without interphase, were observed. The displacement fields required to apply the general solution were obtained by Finite Element Analysis (FEA) performed with a commercial software (ABAQUS 6.13–4). The modeled system consists of a single particle surrounded by the interphase within a polymer region under hydrostatic loading applied on the boundary. The mesh was built by 10-node elements and refined in the transition zone.

### 2.2. Analytical solution for spherical particles

The debonding stress equation for spherical inclusion embedded in an interphase has been already published by Zappalorto *et al* [15]:

$$\sigma_{cr} \cong \sqrt{\frac{4\gamma}{r_p}\frac{E_m}{(1+\upsilon_m)}}\sqrt{\frac{\frac{G_i}{G_m}\left(4+\frac{3K_i}{G_m}\right)-\frac{3K_i}{G_m}\left(\frac{G_i}{G_m}-1\right)\left(\frac{r_p}{r_i}\right)^3}{4+\frac{3K_i}{G_m}+4\left(\frac{G_i}{G_m}-1\right)\left(\frac{r_p}{r_i}\right)^3}} \quad (2)$$

where: $K_k = E_k/(3(1-2\nu_k))$ and $G_k = E_k/(2(1+2\nu_k))$ are the bulk and shear modulus, respectively. While, $E_k$ and $\nu_k$ are the elastic modulus and Poisson's ratio of the components.

## 3. Debonding process analysis

### 3.1. Debonding strength with interphase

The aim of this section is to analyze the relevance of the interphase on the debonding process. The definition of the particle dimensions and shapes was based on the previously reported work [21]. For all of the analyzed geometries, the critical stresses were normalized with the determined strength for the largest filler size (100 $\mu$m) without interphase and plotted as a function of the particle shortest semi-axis.

Figure 2 shows the normalized critical values for spherical particles surrounded by the interphase with the different thicknesses and elastic properties considered. First, a good agreement between analytical and simulated results can be observed for all of the different situations. Taking into account the transition region, a noticeable effect of the elastic properties was detected while on the contrary, the interphase thickness displayed only a marginal influence on the determined critical stresses. Stiffer transitions led to higher critical values while the opposite trend was observed with softer ones. The obtained results for spheres without interphase lay equidistant to these extreme situations. In addition, the observed effect of the transition characteristics is in agreement with already reported data [8, 15].

Normalized debonding stresses for elliptical particles are shown in figure 3. In a similar way as previously described, a more significant influence of the interphase elastic modulus was observed. For small sizes, prolate

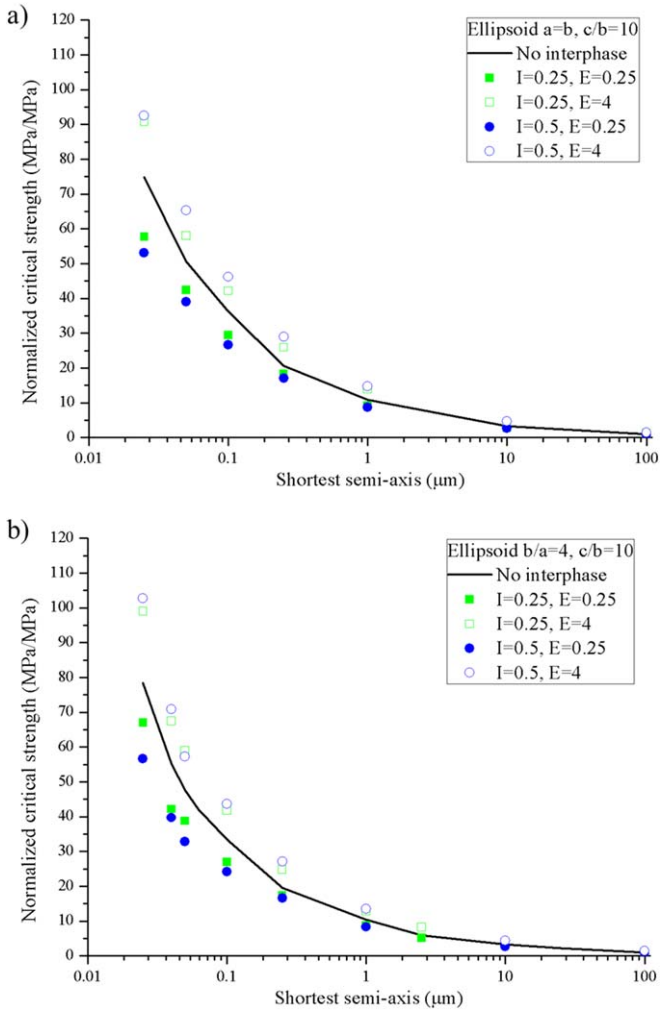


**Figure 3.** Normalized debonding stress values for ellipsoids: (a) prolate and (b) tri-axial.

spheroids (figure 3(a)) exhibited lower stresses compared to tri-axial ellipsoids (figure 3(b)). The calculated values for fibers (figure 4), with square or circular cross-section, also confirmed the predominant effect of the interphase elastic properties independently of the particle geometry considered.

### 3.2. Debonding strength comparison

The determined strengths for the different geometries and transition characteristics were directly compared with the no interphase situation. The largest variations (figure 5(a)) can be observed for the spheres. In this case, the thicker interphase promoted some additional influence on the debonding process. Relative values remained almost constant for all of the other analyzed geometries. It was previously discussed that, energetic and stress criteria are clearly required for accurate predictions [6, 16, 19]. For this reason, the stress concentration factor ($K_t$) before debonding and the energetic change during this process were also determined for each investigated situation. In one hand, the different combination of particle geometries and interphase characteristics can promote large variable stress concentrations around the filler-matrix boundary. On the other hand, debonding process can trigger additional energy consumption mechanisms as plastic void growth or matrix shear yielding [6, 14].

The corresponding $K_t$ values for each filler were normalized with the no interphase system. The relative $K_t$ values (figure 5(b)) with softer transitions were almost constant and lower than the no interphase systems. On the contrary, stiffer transitions exhibited some variations between geometries with a maximal value for fibers (square cross-section). Some particular situations can be analyzed, as for example spherical particles surrounded by stiffer interphase. The $K_t$ values (similar to the no interphase system) in relation with the critical strengths (1.6 higher to the no interphase situation) suggest that, debonding should be achieved at relative higher stress remotely applied. On the contrary, for fiber (square cross-section) the combination of weaker critical strengths with the largest relative $K_t$ values promoted debonding processes at lower applied load.

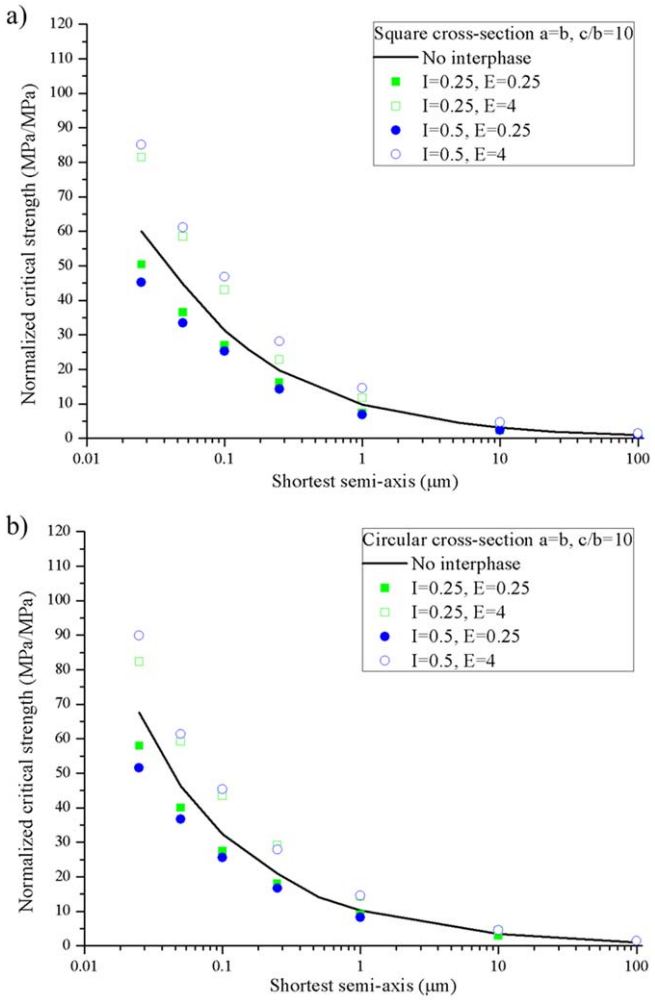


**Figure 4.** Normalized debonding stress values for fibers with different cross-section: (a) square and (b) circular.

The energy variations (figure 5(c)) during debonding of spheres were quite independent of the interphase characteristics. These results clearly differ to the determined critical stress values suggesting an almost constant, at a defined filler size, dissipated energy. On the other hand, prolate spheroids (figure 5(d)) exhibited higher energetic variations with softer transitions compared to the no interphase situation. This performance and the critical stress values suggests that, softer interphase promoted higher energy dissipations at weaker strengths. Similar results were obtained with tri-axial ellipsoids and fibers (not shown here). In addition, it can be remarked that spheres exhibited the lowest dissipated energy, independently of the interphase presence, during the debonding process.

### 3.3. Debonding stress predictions analysis

The size range applicability of the proposed solution should be exhaustively analyzed in order to avoid unrealistic predictions. In this way, a lower limit is clearly required due to the equation could tend to infinity for nano-sized fillers. The strength values have not been experimentally confirmed and this topic can be really helpful for a direct comparison with theoretical predictions. In addition, based on the obtained results above described, the spherical situation showed as the most sensitive. For nano-spheres, the debonding stress was largely increased, particularly with stiff interphase, compared to the other filler geometries. It can be highlighted that, the calculated critical values did not take into account the elasto-plastic matrix behavior. Localized matrix yielding could be a relevant involved factor, directly related to the displacement field around rigid filler.

On the other hand, Carraro *et al* [16] considered the possible transition of the main damage process (matrix failure to debonding) and the trigger parameter of debonding (toughness to strength). They related the slope (critical strength/fiber radius) values close to −0.5 with debonding controlled by fracture toughness. Figure 6 shows a linear regression for spherical particles, as example for the different analyzed situations. The determined characteristic slopes (table 1) for each analyzed situation suggest the predominant effect of the interface fracture toughness.

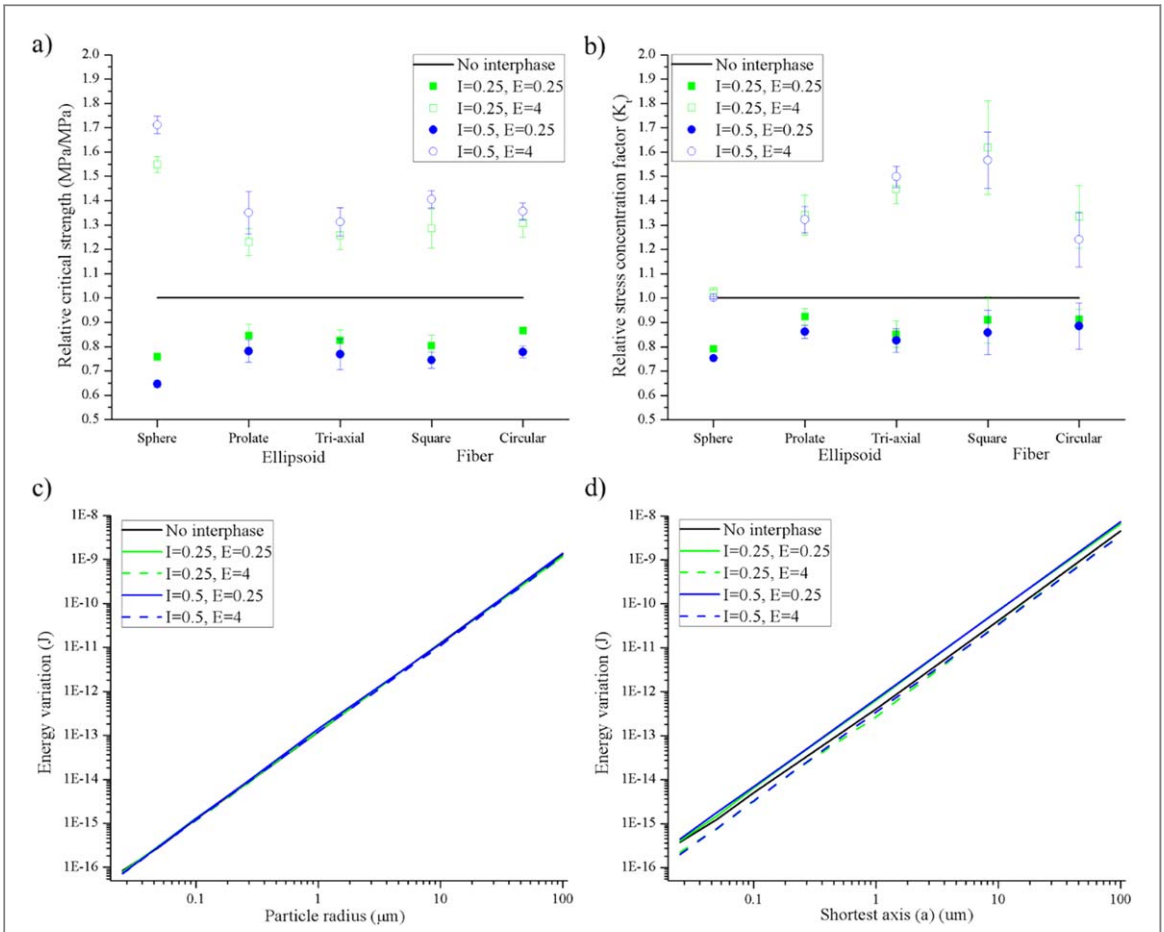


**Figure 5.** Comparison between filler geometries: (a) relative critical strength, (b) relative stress concentration factor ($K_t$) and debonding energy for (c) spheres and (d) prolate ellipsoids.

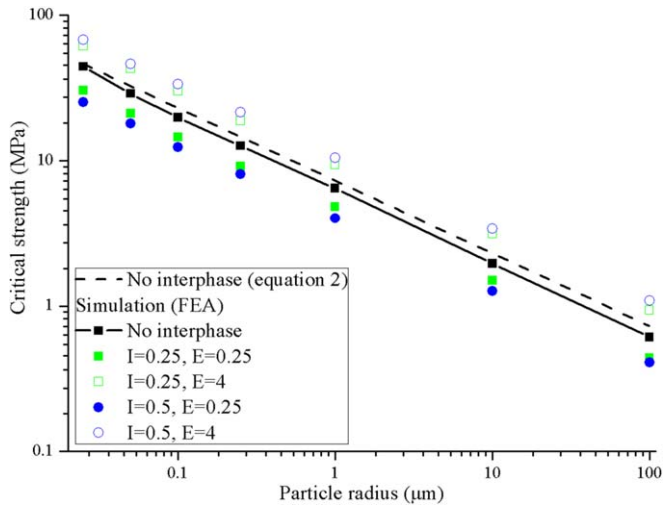


**Figure 6.** Critical strength values for spheres.

## 4. Conclusions

The previously developed equation to determine the particle debonding strength was applied for different fillers surrounded by an interphase. The influence of the transition zone characteristics on the debonding process of rigid fillers was analyzed. The obtained results indicated:

**Table 1.** Slopes for the different particle shapes.

| | | Thickness = 0.25*a | | Thickness = 0.5*a | |
|---|---|---|---|---|---|
| | No interphase | $0.25^{*}E_m$ | $4^{*}E_m$ | $0.25^{*}E_m$ | $4^{*}E_m$ |
| **Sphere** | | | | | |
| a = b = c | −0.50 | −0.50 | −0.50 | −0.49 | −0.49 |
| **Ellipsoid** | | | | | |
| a = b, c/b = 10 | −0.52 | −0.50 | −0.51 | −0.50 | −0.49 |
| b/a = 4, c/b = 10 | −0.51 | −0.52 | −0.52 | −0.49 | −0.51 |
| **Fiber** | | | | | |
| a = b, c/b = 10 (square) | −0.49 | −0.51 | −0.50 | −0.50 | −0.48 |
| a = b, c/b = 10 (circular) | −0.50 | −0.49 | −0.50 | −0.50 | −0.50 |

Note: $r^2 \cong 0.99$ for all of the slopes.

- Softer interphases promoted weaker strengths while the opposite trend was observed for stiffer ones. These performances were detected independently of the filler shape. On the other hand, interphase thickness displayed only a marginal influence.
- The spherical situation whit the different transition zones, displayed the largest variations for the determined strengths. While, on the contrary, this system exhibited the lowest dissipated energy and it was quite independent of the interphase characteristics.
- The critical values for the other geometries remained almost constant, particularly with a softer transition. While, the dissipated energy was enhanced with this soft interphase compared to stiffer ones.

## Acknowledgments

The authors want to acknowledge to the National Scientific and Technical Research Council of Argentina (CONICET) and to the National Institute of Industrial Technology of Argentina (INTI) for the financial support.

## ORCID iDs

E Pérez https://orcid.org/0000-0001-9987-2850

## References

[1] Móczó J and Pukánszky B 2008 Polymer micro and nanocomposites: structure, interactions, properties *J. Ind. Eng. Chem.* **14** 535–63
[2] Sun L, Gibson R F, Gordaninejad F and Suhr J 2009 Energy absorption capability of nanocomposites: a review *Comp. Sc. and Tech.* **69** 2392–409
[3] Fu S Y, Feng X Q, Lauke B and Mai Y W 2008 Effects of particle size, particle/matrix interface adhesion and particle loading on mechanical properties of particulate–polymer composites *Comp.* B **39** 933–61
[4] Thio Y S, Argon A S and Cohen R E 2004 Role of interfacial adhesion strength on toughening polypropylene with rigid particles *Pol.* **45** 3139–47
[5] Cotterell B, Chia J Y H and Hbaieb K 2007 Fracture mechanisms and fracture toughness in semicrystalline polymer nanocomposite *Eng. Frac. Mech.* **74** 1054–78
[6] Williams J G 2010 Particle toughening of polymers by plastic void growth *Comp. Sc. Tech.* **70** 885–91
[7] Deblieck R A C, van Beek D J M, Remerie K and Ward I M 2011 Failure mechanisms in polyolefines: the role of crazing, shear yielding and the entanglement network *Pol.* **52** 2979–90
[8] Salviato M, Zappalorto M and Quaresimin M 2013 Nanoparticle debonding strength: a comprehensive study on interfacial effects *Int. J. Sol. and Str.* **50** 3225–32
[9] Lauke B 2008 On the effect of particle size on fracture toughness of polymer composites *Comp. Sc. Tech.* **68** 3365–72
[10] Quaresimin M, Schulte K, Zappalorto M and Chandrasekaran S 2016 Toughening mechanisms in polymer nanocomposites: from experiments to modelling *Comp. Sc. Tech.* **123** 187–204
[11] Pukánszky B 2005 Interfaces and interphases in multicomponent materials: past, present *Future Eur. Pol. J.* **41** 645–62
[12] Ning N, Fu S, Zhang W, Chen F, Wang K, Deng H, Zhang Q and Fu Q 2012 Realizing the enhancement of interfacial interaction in semicrystalline polymer/filler composites via interfacial crystallization *Prog. Pol. Sc.* **37** 1425–55
[13] Miltner H E, Van Assche G, Pozsgay A, Pukánszky B and Van Mele B 2006 Restricted chain segment mobility in poly(amide) 6/clay nanocomposites evidenced by quasi-isothermal crystallization *Pol.* **47** 826–35
[14] Quaresimin M, Salviato M and Zappalorto M 2014 A multi-scale and multi-mechanism approach for the fracture toughness assessment of polymer nanocomposites *Comp. Sc. Tech.* **91** 16–21
[15] Zappalorto M, Salviato M and Quaresimin M 2011 Influence of the interphase zone on the nanoparticle debonding stress *Comp. Sc. Tech.* **72** 49–55

[16] Carraro P A, Zappalorto M and Quaresimin M 2015 A comprehensive description of interfibre failure in fibre reinforced composites *Theo. App. Frac. Mech.* **79** 91–7
[17] Dastgerdi J N, marquis G and Salimi M 2014 Micromechanical modeling of nanocomposites considering debonding of reinforcements *Comp. Sc. Tech.* **93** 38–45
[18] Quaresimin M, Salviato M and Zappalorto M 2012 Strategies for the assessment of nanocomposite mechanical properties *Comp.* B **43** 2290–7
[19] Leguillon D 2002 Strength or toughness? A criterion for crack onset at a notch *Euro. J. Mech. A/Solids* **21** 61–72
[20] Chen J K, Huang Z P and Zhu J 2007 Size effect on the damage dissipation in nanocomposites *Comp. Sc. Tech.* **67** 2990–6
[21] Pérez E and Lauke B 2017 Calculation of debonding strength at the interface of particles with different shapes and matrix *Comp. Struct.* **167** 262–70
[22] Albdiry M T and Yousif B F 2019 Toughening of brittle polyester with functionalized halloysite nanocomposites *Comp.* B **160** 94–109
[23] Quan D, Pearson R A and Ivankovic A 2018 Interaction of toughening mechanisms in ternary nanocomposites *Pol. Comp.* **39** 3482–96
[24] Ladani R B, Bhasin M, Wub S, Ravindran A R, Ghorbani K, Zhang J, Kinloch A J, Mouritz A P and Wang C H 2018 Fracture and fatigue behaviour of epoxy nanocomposites containing 1D and 2D nanoscale carbon fillers *Eng. Frac. Mech.* **203** 102–14
[25] Wang P H, Sarkar S, Gulgunje P, Verghese N and Kumar S 2018 Fracture mechanism of high impact strength polypropylene containing carbon nanotubes *Pol.* **151** 287–98
[26] Murariu M and Dubois P 2016 PLA composites: from production to properties *Adv. Drug Del. Rev.* **107** 17–46
[27] Pérez E, Alvarez V, Pérez C J and Bernal C 2013 A comparative study of the effect of different rigid fillers on the fracture and failure behavior of polypropylene based composites *Comp.* B **52** 72–83
[28] Park J M, Kim D S and Kim S R 2003 Interfacial properties and microfailure degradation mechanisms of bioabsorbable fibers/poly-l-lactide composites using micromechanical test and nondestructive acoustic emission *Comp. Sc. Tech.* **63** 403–19
[29] Kerekes T W, Lim H, Joe W Y and Yun G J 2019 Characterization of process–deformation/damage property relationship of fused deposition modeling (FDM) 3D-printed specimens *Add. Manuf.* **25** 532–44
[30] Adak N C, Chhetri S, Sabarad S, Roy H, Murmu N C, Samanta P and Kuila T 2019 Direct observation of micro delamination in graphene oxide incorporated carbon fiber/epoxy composite via *in situ* tensile test *Comp. Sci. Tech.* **177** 57–65
[31] Yuan Z N, Chen H, Li J M, Dai B and Zhang W B 2018 *In-Situ* x-ray tomography observation of structure evolution in 1, 3, 5-Triamino-2, 4, 6-Trinitrobenzene based polymer bonded explosive (TATB-PBX) under thermo-mechanical loading *Mat.* **11** 732–44
[32] Rolland H, Saintier N, Wilson P, Merzeau J and Robert G 2017 *In situ* x-ray tomography investigation on damage mechanisms in short glass fibre reinforced thermoplastics: effects of fibre orientation and relative humidity *Comp.* B **109** 170–86